Fundamental insights into the mass transfer via full dislocation loops due to alternative surface cuts

Yi Cui , Zengtao Chen , Yang Ju

PII: S0020-7683(18)30436-0
DOI: https://doi.org/10.1016/j.ijsolstr.2018.11.005
Reference: SAS 10169

To appear in: *International Journal of Solids and Structures*

Please cite this article as: Yi Cui , Zengtao Chen , Yang Ju , Fundamental insights into the mass transfer via full dislocation loops due to alternative surface cuts, *International Journal of Solids and Structures* (2018), doi: https://doi.org/10.1016/j.ijsolstr.2018.11.005

Fundamental insights into the mass transfer via full dislocation loops due to alternative surface cuts

Yi Cui[1*], Zengtao Chen[2], Yang Ju[1]

[1]*Department of Mechanical Science & Engineering, Graduate School of Engineering, Nagoya University, Nagoya 464-8603, Japan*

[2]*Department of Mechanical Engineering, University of Alberta, Edmonton, AB T6G 2G8, Canada*

Abstract

Mass transfer during the formation and emission of a dislocation loop without non-conservative motions can be very tricky. We combine the molecular statics, nonsingular dislocation theory, finite element (FE) method and molecular dynamics (MD) approach to offer new insights. It is proved both theoretically and numerically that the formation and the dynamic emission of a full shear loop can grow a nanovoid. For the first time, a novel approach is proposed to create a shear loop via a hemispherical surface cut by the atomistic simulation. Such a formation process can produce a similar shear loop to that via a flat surface cut, and yet lead to void growth. We incorporate the non-singular dislocation theory into a FE model to calculate the potential energy regarding different surface cuts. Among possible cuts to create a shear loop, the potential energy would favour the one that grows a void under triaxial tension. We show that the arbitrariness regarding the surface cut of dislocation segments should also be recognized during the dynamic emission process. Under triaxial tension, we confirm the mass transfer during the cross-slipping of V-shape shear loops prior to the completion of prismatic loops. By comparison, the uniaxial tension case shows that a V-shape shear loop is not necessarily the precursor of a

* Corresponding author. Tel.: 1-780-258-2778

E-mail address: cui7@ualberta.ca

prismatic loop. Hence, its mass transfer mechanism should be treated differently.

Keywords: Void growth mechanism; molecular dynamics simulation; dislocation loop; material transport

1. Introduction

Void growth via geometrically-necessary dislocations such as prismatic loops and shear loops was proposed to be the primary mechanism under moderate to high strain rate (Lubarda et al. 2004). Since then, void growth via geometrically-necessary dislocations has become a hot topic. Experimental evidences showed slip bands emanating from a growing void, while MD simulation revealed such void growth via shear loop emission (Traiviratana et al. 2008). Even with different crystal orientations (Bringa et al. 2010) and simulation size (Tang et al. 2012), void growth under uniaxial tension is primary due to the nucleation of shear loops. Potirniche et al. (2006) reported dislocation nucleation due to stress concentration in void-embedded thin film of Face-Centered Cubic (FCC) nickel, which immediately increases void size. Later, Cui and Chen (2015a, 2015b) revealed that those nucleated dislocations in a thin film of FCC metal are primarily incomplete shear loops. The emission of incipient shear loops should occur from the surface of the cylindrical nanovoid, once the image attraction from the void is balanced by the applied load (Lubarda 2011). Krasnikov and Mayer (2015) observed that incomplete shear loops can grow the void by drawing displacement vectors of individual atoms on the void surface. Even under shock loading condition, mass transfer via incomplete shear loops is the primary mechanism for void shrinkage (Xiang et al. 2017). Interestingly, these incomplete shear loops from shock loading can form frustum-like dislocation structures that remarkably resemble those reported elsewhere (Cui and Chen 2016, Cui and Chen 2017c). Most recently, Jing et al. (2018) observed and explained the void growth as the absorption or exit of edge segments (belonging to

incomplete shear loops). This nucleation of shear loop is not limited to void-embedded cases. Rather, it appears a general mechanism regarding FCC metals. Even for an initially defect-free case, such shear dislocation loops can be nucleated homogeneously (Salehinia and Bahr 2014). Similar edge segments or partial shear loops can also be nucleated from grain boundaries (Spearot et al. 2007, Tschopp and McDowell 2008). Thus, the understanding of void growth via geometrically-necessary dislocations should help in the design of structure or nanomaterials with improved integrity or advanced function. For example, nanovoids could act as sinks for better radiation resistance (Bringa et al. 2011). Meng and Jin (2011) showed that the growth of nanowires and nanotubes can be driven by screw dislocations, since they generate surface steps. Hence, the mass transfer mechanism of shear loops, which contain screw segments, may also provide new ideas to nanofabrication.

Despite these overwhelming evidences supporting Lubarda et al. (2004), there appear strong theoretical challenges that deserve to be brought up in the very beginning of the paper:

1. How can shear loops or edge segments, whose Burgers vector is in the loop plane, transfer mass out of/into the void? Would this violate mass conservation (Bulatov et al. 2010)? Besides, what is the difference in mass transfer between a shear loop and a prismatic loop? How should we evaluate the pertinent mass transfer?
2. In the dynamic case, if the shear loop is gradually emitted, would the mass transfer be zero since the area swept by the dislocation segment is only inside the gliding plane (zero projected area onto the Burgers vector)?
3. Must the amount of mass transferred be forfeited upon the completion of a full shear loop?
4. Are V-shape shear loops able to grow void only because they are precursors of prismatic loops?

These questions are seemingly simple yet unexpectedly tricky. Questions 1 will be answered in section 2, while question 2-4 will be answered in section 3. Compared with our previous work, this paper brings brand-new insights, which is organized as follow. Section 2 describes a control volume-based approach to evaluate the mass transfer via geometrically-necessary dislocations like full shear loops. By comparison, only incomplete shear loops have been considered previously. Besides, we will shed light on the energetics associated with different surface cuts. The most likely surface cut under external load will thus be determined. Two kinds of atomistic simulations are involved. The first kind of simulation in section 2 applies the "cut, displace and paste" operation to create a full shear loop. Both the arbitrariness of the surface cut and the related void growth can thus be examined. To our best knowledge, such arbitrariness in creating a dislocation loop has never been reported before. The second kind of simulation in section 3 focuses on the dynamic emission of shear loops and prismatic loops from initially dislocation-free matrix under external load. Improved analysis on V-shape shear loops could better capture the mass transfer during their evolution. The visualization method of mass transfer will also be validated by the void growth via prismatic loops. The ongoing mass transfer during the conversion of V-shape loops into prismatic loops will be examined and should offer critical insights to aforementioned challenges.

2. The quasi-static formation

2.1 New theoretical insights

The mass transport associated with geometrically necessary dislocations requires nontrivial understanding. The key fact is that the surface cut to create them can be arbitrary. We start with edge dislocation segments. Fig. 1 depicts three possible cuts for an edge dislocation segment. A prismatic loop only consists of edge segments, while s shear loop also contains edge, screw and

mixed segments. Both the prismatic loop and the shear loop can be created by a surface cut in their loop plane, which everyone should agree with. However, this rather leads to a less commonly accepted idea that an edge segment can have different surface cuts such as the vertical one in Fig. 1(a) or the horizontal one in Fig. 1(b). In fact, this precisely reflects which was proposed by Hirth and Lothe (1982) that a surface cut for an edge dislocation can be arbitrary as in Fig. 1(c). Another worth noting fact is that the surface cut and the possible gliding cylinder are not necessary in the same plane as seen in Fig. 1(a). Therefore, a surface cut of a shear loop can be outside its gliding plane. In fact, they should be unrelated due to arbitrariness, although they can sometimes and very often be in a same plane as seen in Fig. 1(b).

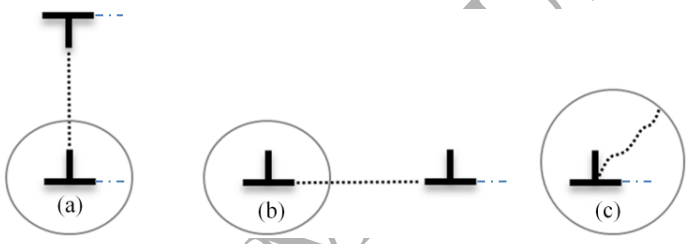

Fig.1 Cross-sectional views of edge segments belonging to (a) a prismatic loop and (b) a shear loop, assuming both are created by a flat surface cut (short black dash). Figure (c) shows an edge segment created by an arbitrary cut (Hirth and Lothe 1982). Figure (a) shows that surface cut plane and the gliding plane are not necessarily the same.

Since a shear loop contain edge segments, its surface cut should certainly be arbitrary too. To the stress field or strain energy of a complete shear loop, this arbitrariness can be eliminated by using Stokes' theorem. In sharp contrast, to mass transport, this arbitrariness is not eliminable by either Stokes' or Gauss' theorem. Since most of the previous researches focused on the stress field or strain energy of a dislocation loop, this arbitrariness was routinely ignored for the sake of simplicity yet without any problem. However, it is not the case for mass transport. Special attention should be paid to this arbitrariness regarding the formation and dynamic emission of

geometrically-necessary dislocations, especially shear loops. In fact, this arbitrariness has been acknowledged in at least three textbooks (Landau Lifshitz 1970, Hirth and Lothe 1982, Bower 2009). According to Hirth and Lothe (1982), the following equation is for the amount of material to be removed or inserted for creating a dislocation loop.

$$\Delta V = \int_A \mathbf{b} \cdot \mathbf{n} \mathrm{d}S \tag{1}$$

One should never exclusively choose A as the flat one, which forces the integrand $\boldsymbol{b} \cdot \boldsymbol{n}$ ($\boldsymbol{b}$ is the Burgers vector and $\mathbf{n}$ is the surface norm) to be zero and fundamentally prohibits any local growth by the shear loop. Instead, the arbitrariness should always be respected when dealing with the mass transfer. The operation to create a dislocation loop is understood as follow (Hirth and Lothe 1982). In Fig. 2(a), one displaces the negative side of the arbitrary surface cut A by b relative to the positive side, and then pastes the surface together. A complete dislocation loop is then created, while the surface A becomes prefect again. For a shear loop, this surface cut A should remain arbitrary; otherwise the definition should read "depending on the Burgers vector" instead of "being arbitrary". By respecting this fact, we immediately have the integrand $\mathbf{b} \cdot \mathbf{n} \neq 0$ on most locations of A.

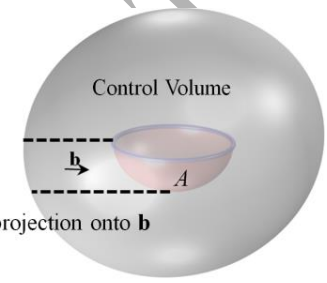

(a) Control volume enclosing a shear loop

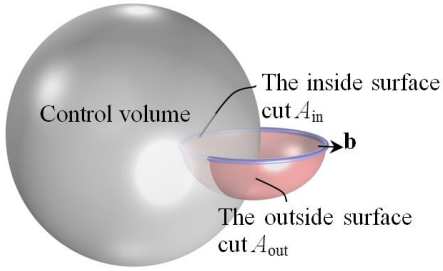

(b) Control volume intersecting a shear loop

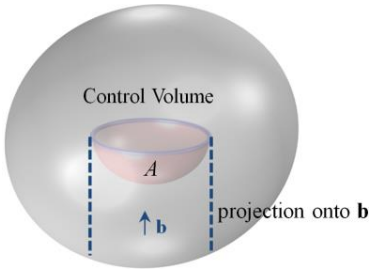

(c) Control volume enclosing a prismatic loop

Fig. 2 Control volumes and dislocation loops created by hemispherical cuts. The control volume here is not a void, but a certain material domain. The control volume in (a) has no mass flow, while those in (b,c) have.

To rigorously evaluate mass transfer, let us first denote the measure for displacement, strain and stress, as $[\boldsymbol{u}^D, \boldsymbol{\varepsilon}^D, \boldsymbol{\sigma}^D]$ respectively, which is induced by dislocations but with zero external load. For a control volume V_{CV} overlapping with the full shear loop and its surface cut in Fig. 2(b), its volumetric change should be

$$\Delta V_{CV} = \int_{\partial V_{CV}} \boldsymbol{u}^D \cdot \boldsymbol{n} \mathrm{d}S \,, \tag{2}$$

By applying Gauss's theorem to the control volume, we obtain

$$\Delta V_{CV} = \int_{V_{CV}} \nabla \cdot \boldsymbol{u}^D \mathrm{d}V \,. \tag{3}$$

The divergence of the displacement is the sum of the trace of elastic strain and that of the eigenstrain due to dislocation:

$$\Delta V_{CV} = \int_{V_{CV}} \varepsilon_{kk}^{el} \mathrm{d}V + \int_{V_{CV}} \varepsilon_{kk}^{*} \mathrm{d}V \,, \tag{4}$$

where both the elastic strain and the eigenstrain could contribute. For the shear loop in Fig. 2(b), the plastic eigenstrain takes the form (Landau Lifshitz 1970)

$$\varepsilon_{ij}^{*}(\boldsymbol{x}) = -\tfrac{1}{2}(b_i n_j + b_j n_i)\delta(\boldsymbol{A}_{in} - \boldsymbol{x}) \,, \tag{5}$$

where $\boldsymbol{A}=\boldsymbol{A}_{\mathrm{in}}+\boldsymbol{A}_{\mathrm{out}}$ denotes total surface cut and $\boldsymbol{A}_{\mathrm{in}}$ the part inside this control volume, b_i is the

component of the Burgers vector and $\delta(\boldsymbol{A}_{in}-\boldsymbol{x})$ is the Dirac function in the normal direction of the surface. By substituting Eq. (5) and ignoring the elastic growth, the volumetric change of the control volume in Fig. 2(b) should be nonzero:

$$\Delta V_{CV}^{*}=\int_{V_{CV}}\varepsilon_{kk}^{*}\mathrm{d}V=-\int_{A_{in}}\boldsymbol{b}\cdot\boldsymbol{n}\mathrm{d}S=\int_{A_{out}}\boldsymbol{b}\cdot\boldsymbol{n}\mathrm{d}S\neq 0. \tag{6}$$

By comparison, since the whole $\boldsymbol{A}=\boldsymbol{A}_{\mathrm{in}}+\boldsymbol{A}_{\mathrm{out}}$ is enclosed in Fig. 2(a), there is no volumetric change to this control volume:

$$\int_{A_{in}+A_{out}}\boldsymbol{b}\cdot\boldsymbol{n}\mathrm{d}S=0. \tag{7}$$

Hence for the shear loop, the control volume in Fig. 2(b) has 'mass flow' in or out. Despite of the gross zero in Eq. (7) for Fig. 2(a), mass has been redistributed inside. Indeed, for the material inside the dome-shape A, there should have mass transfer. By comparison, any control volume, as long as it encloses a prismatic loop, will always have volumetric change. In other words, the mass transfer is local for a shear loop, while nonlocal for a prismatic loop.

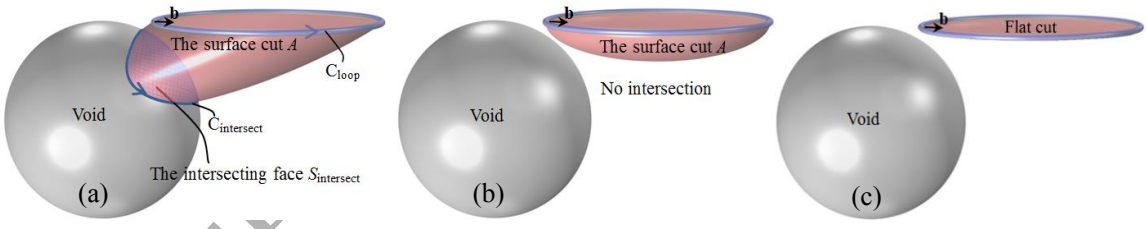

Fig. 3 A full shear loop with void growth in (a) and without void growth in (b, c). The surface cut A, by definition, should be inside the material. In (a), $C_{\mathrm{intersect}}$ is only the intersection between the surface cut A and the void surface. Hence, $S_{\mathrm{intersect}}$ is not a part of surface cut since it only has material on one side, whose bounding curve $C_{\mathrm{intersect}}$ is not a dislocation loop. For clarification, the C_{loop} was not emitted from the location of $C_{\mathrm{intersect}}$. Fig. 1 has already clarified that surface cut plane and the gliding plane are not necessarily the same.

Figures 3(a, b) show a nonflat surface cut with and without intersection, while Fig. 3(c) shows

a flat surface cut. For the complete shear loop in Fig. 3(a), the same approach applies and the void growth should be nonzero:

$$\Delta V_{void}^{*} = -\int_{V_{matrix}} \varepsilon_{kk}^{*} \mathrm{d}V = \int_{A} \boldsymbol{b}\cdot\boldsymbol{n}\mathrm{d}S = -\int_{S_{\text{intersect}}} \boldsymbol{b}\cdot\boldsymbol{n}\mathrm{d}S \neq 0\,, \tag{8}$$

where A denotes the elongated surface cut in Fig. 3(a). By comparison, if no intersection between void and the surface cut, there would be no void growth. Furthermore, Eq. (8) will later be verified by the atomistic simulation in the upcoming section.

2.2 Potential energies evaluated by finite element method

This arbitrariness gives rise to another question: among all the possible surface cuts to create a shear loop near a void, which one could be favoured by the principle of minimum potential energy? Such an analysis could be nontrivial, which requires FE method to solve for the image stress regarding different cuts. Meanwhile, classical dislocation theory would cause singularity along the loop. As a result, the non-singular dislocation theory is better to be incorporated into the FE calculation.

To start, let us denote two measures of displacement, strain and stress: the fields induced by the applied load in a dislocation-free solid $[\boldsymbol{u}^{\boldsymbol{Ext}}, \boldsymbol{\varepsilon}^{\boldsymbol{Ext}}, \boldsymbol{\sigma}^{\boldsymbol{Ext}}]$ and the fields induced by dislocations but with zero external load $[\boldsymbol{u}^{D}, \boldsymbol{\varepsilon}^{D}, \boldsymbol{\sigma}^{D}]$ (Bower 2009). Both sets of fields satisfy traction-free condition on void surface. The total displacement, stress and strain fields are the superposition of the two. The total potential energy of a void-embedded solid under external loading can be expressed as (Bower 2009)

$$\Pi = \Pi^{D\infty} + \Pi^{I} + \Pi^{D^{Ext}} + \Pi^{Ext}\,, \tag{9}$$

The strain energy of a standalone dislocation is

$$\Pi^{D\infty} = -\int_A \frac{1}{2}\sigma_{ij}^{D} b_i n_j dS \,. \tag{10}$$

The minus sign is due to flipped surface normal direction (Hirth and Lothe 1982). The work done to introduce the dislocation into the external load $\boldsymbol{\sigma^{Ext}}$ is

$$\Pi^{D^{Ext}} = -\int_A \sigma_{ij}^{Ext} b_i n_j dS + \int_{A_{Void}} \sigma_{ij}^{Ext} u_i^{D} n_j dS \,. \tag{11}$$

Again, the minus sign is due to the flipped surface normal direction. It is worth noting that we here not only take the surface effect of the nanovoid into the consideration (Sharma, 2003), but also respect the fact the displacement caused by the dislocation should be nonzero at the nearby void surface. Since this displacement is a second-order infinitesimal with respect to the distance away from the cut (Landau and Lifshitz 1970), the second term could be relatively insignificant. The displacement due to dislocations consists of two parts:

$$u_i^{D} = u_i^{D\infty} + u_i^{I} \tag{12}$$

The first one is given by the Burgers displacement equation below, while the second one is caused by the image effect of void and will be solved numerically.

$$\boldsymbol{u}^{D\infty}(\boldsymbol{r}) = \frac{\boldsymbol{b}}{4\pi}\int_A \frac{(\boldsymbol{r}'-\boldsymbol{r})\cdot \mathrm{d}\boldsymbol{S}}{|\boldsymbol{r}'-\boldsymbol{r}|^3} - \frac{1}{4\pi}\oint_C \frac{\boldsymbol{b}\times \mathrm{d}\boldsymbol{l}'}{|\boldsymbol{r}'-\boldsymbol{r}|} + \frac{1}{8\pi(1-\nu)}\, grad \oint_C \frac{[\boldsymbol{b}\times(\boldsymbol{r}'-\boldsymbol{r})]\cdot \mathrm{d}\boldsymbol{l}'}{|\boldsymbol{r}'-\boldsymbol{r}|}, \tag{13}$$

where $\boldsymbol{r}$ is the radial vector of the point concerned, $\boldsymbol{r}'$ is the radial vector of the points either on area A or its bounding curve C to perform the integration, $\mathrm{d}\boldsymbol{l}'$ is the differential line element and ν is the Poisson ratio.

The change in potential energy by the image stress due to void is

$$\Pi^{I} = -\int_A \sigma_{ij}^{I} b_i n_j \mathrm{d}S \,. \tag{14}$$

The last is the potential energy of the applied load itself in an undislocated solid, which is independent of surface cuts ($\mathrm{d}\tau$ is the differential volumetric element).

$$\Pi^{Ext} = \int_R \sigma_{ij}^{Ext} \varepsilon_{ij}^{Ext} \mathrm{d}\tau - \int_{\partial R} t_i u_i^{Ext} \mathrm{d}S\,, \tag{15}$$

For a standalone dislocation loop C, its strain energy can be converted into a line integral (Cai et al. 2006, Bower 2009).

$$\begin{aligned}\Pi^{D\infty} = &-\frac{\mu}{8\pi}\oint_C\oint_C \frac{\partial^2 R_\rho}{\partial x_k \partial x_k} b_i b_j \mathrm{d}x_i \mathrm{d}x_j' - \frac{\mu}{4\pi(1-\nu)}\oint_C\oint_C \frac{\partial^2 R_\rho}{\partial x_i \partial x_j} b_i b_j \mathrm{d}x_k \mathrm{d}x_k' \\ &+ \frac{\mu}{4\pi(1-\nu)}\left[\oint_C\oint_C \frac{\partial^2 R_\rho}{\partial x_k \partial x_k} b_i b_i \mathrm{d}x_j \mathrm{d}x_j' - \nu\oint_C\oint_C \frac{\partial^2 R_\rho}{\partial x_k \partial x_k} b_i b_j \mathrm{d}x_j \mathrm{d}x_i'\right]\end{aligned}, \tag{16}$$

where μ is the shear modulus. To remove the singularity along the curve, the nonsingular dislocation theory is applied here, which resembles classical expressions except that the displacement vector is modified as $R_\rho(\mathbf{x}) = \sqrt{x_k x_k + \rho^2}$. If taking the shape in Fig. 3(a), the surface A will be bounded by two curves: the loop and the intersection curves. Hence, Stokes' theorem is applicable to the strain energy and Eq. (16) is still valid. Yet, the line integral should not only concern the loop curve, since the arbitrary surface cut could carve an arbitrary intersection curve on the void surface. Respecting the direction of the two curves in Fig. 3(a), we have:

$$C = C_{loop} - C_{intersect}\,. \tag{17}$$

In a similar fashion, the stress due to dislocation loop is modified as:

$$\begin{aligned}\sigma_{ij}^D = &\frac{\mu}{8\pi}\oint_C \frac{\partial^3 B_\rho}{\partial x_\alpha \partial x_p \partial x_p}[\in_{\alpha mi} b_m \mathrm{d}x_j' + \in_{\alpha mj} b_m \mathrm{d}x_i'] \\ &+ \frac{\mu}{4\pi(1-\nu)}\oint_C \in_{\alpha mk} b_m \left(\frac{\partial^3 B_\rho}{\partial x_\alpha \partial x_i \partial x_j} - \delta_{ij}\frac{\partial^3 B_\rho}{\partial x_\alpha \partial x_p \partial x_p}\right)\mathrm{d}x_k'\end{aligned}, \tag{18}$$

where $\in_{\alpha mk}$ is the permutation tensor. The function $B_\rho(\mathbf{x}) = (1-m)\sqrt{x_k x_k + \rho_1^2} + m\sqrt{x_k x_k + \rho_2^2}$ is designed to remove singularity near the dislocation core by convolution, where $\rho_1 = 0.9038\rho$,

$\rho_2 = 0.5451\rho$ with the cut-off distance ρ to be determined later and the fitting coefficient $m = 0.6575$. If dislocation motion were to be considered, a second convolution of Eq. (18) should be taken, which converts $B_\rho(\mathbf{x})$ into $R_\rho(\mathbf{x})$. Since the aim here is to compute the image stress, the second convolution is not needed. Nevertheless, the strain energy of a circular shear loop, by numerically integrating Eq. (16), will be compared with that given by Cai el al. (2006). The same treatment will be applied to Eq. (13) to eliminate the singularity in calculating $\Pi^{D^{Ext}}$.

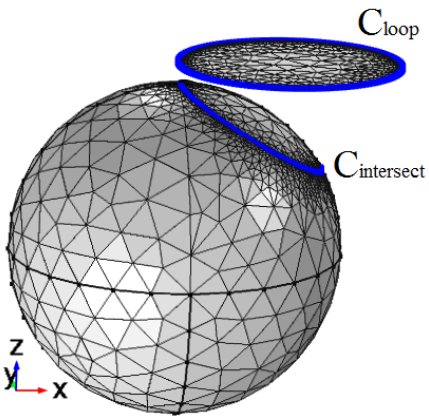

Fig. 4 The meshed FE model. The hemispherical surface cut is not shown.

The total stress, due to the presence of void, must satisfy the traction-free boundary condition on the void surface. Hence, the image stress must satisfy:

$$\boldsymbol{\sigma}^I \cdot \mathbf{n} + \boldsymbol{\sigma}^D \cdot \mathbf{n} = 0 \qquad \text{on void surface} \qquad (19)$$

Even if the size effect of nanovoid is to be considered, Eq. (19) remains the same since the surface tension can be treated as a surface load. Once knowing the stress generated by the dislocation, the image stress can be obtained through solving the stress equilibrium equation numerically. In this way, the non-singular dislocation theory is incorporated into the finite element calculation. The center of the circular shear loop (R_{loop}=8.5nm) coincides with the center of a cubic material domain (85nm×85nm×85nm). The spherical void (R_0=12.75nm) is centered at (-8.5nm, 0nm, 14.45nm). The elastic constants applied in the calculation are E=120 GPa and v

=0.33 for bulk copper. The calculation takes two steps. The first step is to obtain the surface stress due to the presence of dislocation and the second step is to obtain image stress. Void surface is meshed with triangular elements. No volumetric mesh is needed at the first step. Inside the material domain, only the void and the surface cut as shown in Fig. 4 are meshed. Numerical line integration along C_{loop} for the flat cut (C_{loop} and $C_{inersect}$ for the hemispherical cut) is carried out to evaluate the surface stress and the result is saved. At step 1, the number of triangular elements meshed on the surface cut is 2632. At step 2, the material domain is meshed with tetrahedral elements. The stress on void surface from step 1 serves as the surface load for the domain calculation. Along with periodic boundary condition, the image stress field in the domain is then obtained by the FE method. The shape function is quadratic. In step 2, the total number of the tetrahedral elements is 199092. The minimum element length of local refinement surrounding the dislocation line is 0.68 nm. The dislocation line is meshed with 0.255 nanometer-length edge elements. The mesh strategy is based on extensive mesh convergence tests. The numerical integration is performed with an integration order of 4. The numerically-integrated fields (displacement, strain and stress) induced by dislocations is first validated by those derived from the classical analytical solution (Ohr 1972) by setting $\rho = 0$. Further, the nonsingular strain energy for a circular dislocation loop is validated by the nonsingular dislocation theory (Cai et al. 2006), which reads:

$$\Pi_{ana}^{\infty} = 2\pi R \frac{\mu b^2}{8\pi}\left[\frac{2-\nu}{1-\nu}\left(\ln\frac{8R}{\rho}-2\right)+\frac{1}{2}\right]+\mathrm{O}\left(\frac{\rho^2}{R^2}\right), \tag{20}$$

where R is the radius of the loop and ρ is the cut-off distance. Any cut without intersecting the void is the same to the flat cut, since both its stress and strain energy can be fully converted into a line integral that only concerns the loop itself. A good agreement between $\Pi^{D\infty}$ and $\Pi_{ana}^{D\infty}$ can

be seen from Table 1 for the flat surface cut with different core cut-off ρ. Interestingly, take ρ=b for example, $\Pi^{I}+\Pi^{D\infty}$ of the flat cut is almost the same to that of the hemispherical cut as seen in Table 1. Additional calculations with differently-sized or elongated hemispheres confirmed this issue (not shown for brevity). Without considering the external load, which annihilates the term $\Pi^{D^{Ext}}+\Pi^{Ext}$, a flat cut and a hemispherical cut are equally likely. That is to say, the sum of these two terms almost stay the same for the two different cuts. As seen in Table 1, different cut-off distances ρ barely affect this conclusion.

Table 1

Potential energies by FE calculation for different surface cuts. Any cut without intersecting the void is same to the flat cut. The magnitude of Burgers vector is 0.255 nm for a perfect dislocation in FCC copper.

Different cut-off:	$\rho=b$		$\rho=2b$	
Surface cut:	Flat	Hemispherical	Flat	Hemispherical
Π^{I}(eV)	-20.000	-220.75	-19.894	-171.07
$\Pi^{D\infty}$ (eV)	360.72	562.41	293.81	443.38
$\Pi^{D\infty}_{ana}$ (eV)	367.22		300.00	
$\Pi^{I}+\Pi^{D\infty}$(eV)	340.72	341.66	273.92	272.31

Since the fourth term Π^{Ext} in the total potential energy is for the undislocated configuration, it should be the same for any surface cut. The remaining term that truly matters is thus only $\Pi^{D^{Ext}}$, which is the work done to introduce the dislocation under the external load. Assuming a nearly equal triaxial tension $\sigma_{ij}^{Ext}\approx\sigma\delta_{ij}$ and neglecting the second term in Eq. (11), it is intuitive to see that

$$\Pi^{D^{Ext}}\approx-\sigma\int_{A}\mathbf{b}\cdot\mathbf{n}dS=-\sigma\Delta V\,. \tag{21}$$

Obviously, $\Delta V > 0$ is more energetically favourable than $\Delta V = 0$. For prismatic loops, this leads to the well-known understanding that their formation under triaxial load causes voids to grow. Similarly, the hemispherical surface cut as shown in the inset of Fig. 5 would be favoured under triaxial tension. Due to the presence of void and the anisotropy of the crystalline, the shear stress at certain slip plane can induce dislocations under triaxial loading, which is well-known. Next, we consider the image effect and the surface effect due to the nanovoid (Sharma, 2003).

$$\sigma_{rr} = -\frac{4\mu\sigma^{\infty}}{3K}\left(\frac{3K+4\mu-2\tau_0/R_0}{4\mu+2K_s/R_0}-1\right)\frac{R_0^3}{r^3}+\sigma^{\infty} \tag{22}$$

$$\sigma_{\theta\theta} = \sigma_{\phi\phi} = \frac{2\mu\sigma^{\infty}}{3K}\left(\frac{3K+4\mu-2\tau_0/R_0}{4\mu+2K_s/R_0}-1\right)\frac{R_0^3}{r^3}+\sigma^{\infty} \tag{23}$$

The stress components are written in spherical coordinates. The parameter μ is the shear modulus, K is the bulk modulus, K_S=12.932 N/m is the surface modulus for [1 1 1] crystal direction (Sharma et al. 2003, Zhao et al. 2014), R_0 is the radius of nanovoid, τ_0 is residual surface tension (Sharma et al. 2003) and σ^{∞} is the remote triaxial stress. Such treatment introduced the intrinsic size to the classical elasticity theory. The size effect of the nanovoid induces a surface tension, which can be viewed as an additional load on the void surface. The resulted stress field is no long an equal-triaxial one, yet Eq. (21) can still be helpful for an intuitive understanding.

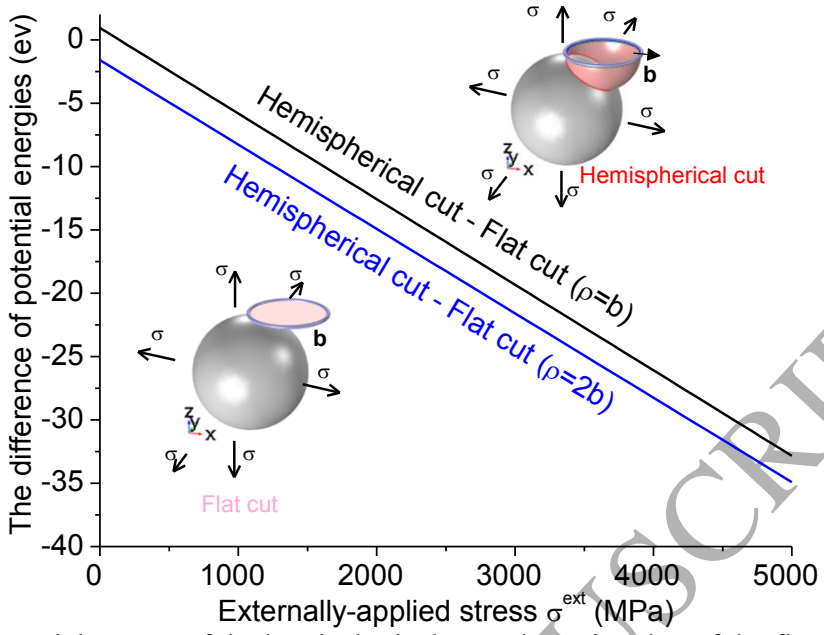

Fig. 5 The potential energy of the hemispherical cut subtracting that of the flat cut versus the external triaxial stress. Surface cuts without intersecting the void are the same to the flat cut. The potential energy of the load itself is irrelevant to the dislocations.

Fig. 5 indicates that the potential energy with the image effect and the size effect would still favour the hemispherical surface cut that grows the void under remote triaxial tension. Further, the larger the external stress is, the more the hemispherical cut could be favoured as seen in Fig. 5. Different cut-off distances ρ barely affect this conclusion in Fig. 5.

2.3 The quasi-static atomistic simulation

In reality, the nucleation of dislocation loops can be either homogeneous inside the material or heterogeneous at some surface (Hirth and Lothe 1982). Full dislocation loops can appear without incomplete ones being precursors. Indeed, the seemingly abstract operation to create a full dislocation loop (Hirth and Lothe 1982) is not unrealistic at all. The critical resolved shear stress for either homogeneous or heterogeneous nucleation could depend on temperature or the type of dislocation (Hirth and Lothe 1982). Other factors such as crystalline orientation could also play a

role in nucleation (Lubarda 2011). Narayan and Washburn (1972) introduced dislocation loop by plastic deformation near free surfaces as seen in Fig. 6. Once these dislocation loops situate beyond a critical distance from surfaces, they would not move. Homogeneous nucleation of shear dislocation loops in a defect-free FCC crystal was also reported by the atomistic simulation (Salehinia and Bahr 2014). Besides, the introduction of dislocation loops is the first step to study related configuration, energy, mobility and interaction with other defects (Li et al. 2015). Therefore, reliable and physical approaches to introduce dislocation loops into un-dislocated solid are of great scientific importance and continue to progress (Dang et al. 2017). Our focus here is the accompanying mass transfer, which has rarely been considered before.

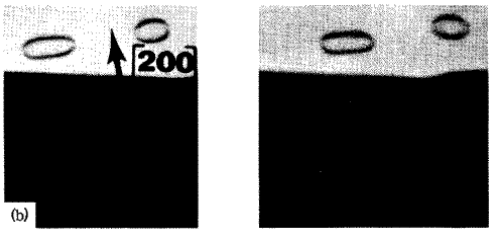

Fig. 6 Dislocation loops created by plastic deformation near a free surface (Reprinted with permission from Narayan and Washburn 1972. Copyright 1972, AIP Publishing LLC).

The preceding section clarified the fact that the generation of a shear loop can induce void growth, depending on the surface cut. The "cut, displace and paste" operation proposed by Hirth and Lothe (1982) is theoretically sound. However, experimentally, it appears unlikely to control surface cuts. Besides, examining arbitrary cuts appears unachievable to the transmission electron microscope, since the scale is beyond the local core structure. For atomistic simulations, things become much easier. We can exactly control the surface cut. A flat surface cut can certainly generate a shear dislocation loop (Dang et al. 2017). If the cut is exclusively chosen as the flat one, there would be no need for the "paste" operation and consequently no mass transfer. Hence, we only need to examine the case of non-flat surface cuts. Since the scope of this work is limited

to the formation rather the evolution of dislocation loops, no external stress is applied to evolve the loop.

Actually, a non-flat surface cut to generate a shear dislocation loop has been reported inadvertently. Zhou et al. (2012) created a shear loop by uniformly displacing atoms within hexagonal cylindrical region over a simulation period of 0.1 ns. Notably, this uniform displacement of atoms is not equivalent to the elastic deformation of a shear loop created by a flat cut. The latter one should be a second-order infinitesimal with respect to the distance away from the cut (Landau and Lifshitz 1970). To a control volume or a void overlapping with the hexagonal cylindrical region, such creation of a dislocation loop would grow or shrink it. For the first time, our atomistic simulation below aims to reproduce the operation proposed by Hirth and Lothe (1982) regarding the arbitrariness.

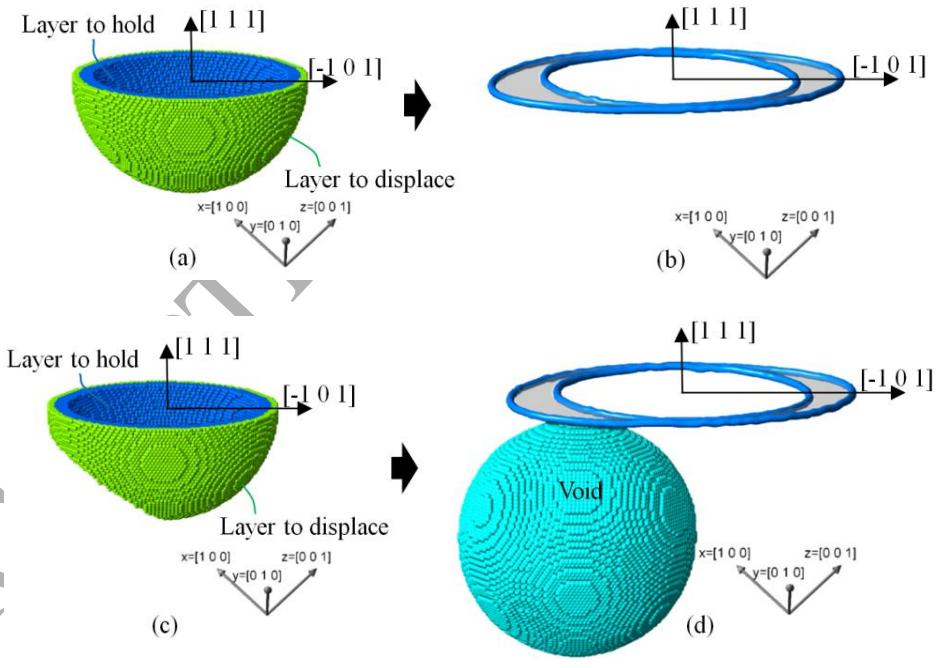

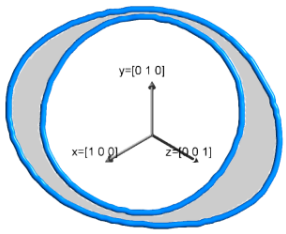

(e) View from [1 1 1] direction of (b)

Fig. 7 The hemispherical surface cut (green outlayer and dark-blue inner layer) in (a) creates a standalone shear dislocation loop in (b). The same surface cut yet missing a piece in (c) creates a shear dislocation loop in (d) near a void. The rendered blue lines represent dislocation curves, while the gray areas represent stacking fault areas. The light blue atoms represent void surface. All other atoms are made invisible. Figure (e) remarkably resembles that generated by a flat cut in Fig. 5 of Dang et al. (2017).

The proposed atomistic simulation to reproduce the operation regarding arbitrary cuts can be summarized as follow.

1. To start, the simulation box (49.9nm×49.9nm×49.9nm) is first filled with face-centered cubic (FCC) copper atoms. The total atom count is roughly 10 million. The ratio of the box length to the radius of dislocation loop is bigger than 6, which helps converge the long-range stress field to that of an infinitesimal loop (Dang et al. 2017). Since the cut is non-flat, this ratio is applied in all three directions. The x, y and z directions align with the [1 0 0], [0 1 0] and [0 0 1] crystal orientations, respectively. Periodic boundaries are adopted for all three directions. This simple orientation gives better result in periodicity. The periodicity ensures that the void is the only free surface. The standalone case in Figs. 7(a, b) contains no void. The case in Figs. 7(c, d) introduces a void of diameter 14.46nm, centered at (25.98nm, 21.32nm, 16.67nm) measured from the corner of the box. All simulations are carried out by Large-scale Atomic/Molecular Massively Parallel

Simulator (LAMMPS) and the Mishin's embedded atom method (EAM) potential for copper (Mishin et al. 2001) is applied throughout the paper. The series of potentials developed by Mishin and his co-authors show better agreement with experiments in several aspects (Dang et al. 2017). After the dislocation-free geometries are created, energy minimization using the conjugate gradient method is performed.

2. The cut operation is translated into identifying atoms constituting the surface cut layer, which cannot be infinitely thin in atomistic simulations. Take the void-free case for example, two layers of atoms are involved in Fig. 7(a). The green, outer hemispherical shell is of inner diameter 14.46nm and outer diameter 15.33 nm. The blue, inner hemispherical shell is of inner diameter 12.72 nm and outer diameter 14.46nm. They share the same center with the simulation box. The green one outside (negative side) is to displace, while the blue one inside is to hold. As a tip to only use built-in commands of LAMMPS, one can create an almost infinitely-large sphere, through manipulating its sphere center, to intersect a small sphere for an arbitrarily-rotated hemispherical shell.
3. The move command of LAMMPS is used to gradually displace atoms at a constant rate to their final positions. The displacement vector is 1/2[-1 0 1], the Burgers vector of a perfect dislocation in FCC metal. The simulation is run under the NVT ensemble at 0.1K for 20000 time step with 1fs for each step. The NVT ensemble is imposed on the atoms excluding those in two layers. The near-zero temperature prevents thermal activation and limits thermal vibration of atoms. The simulation run allows the system to attain elastic deformation to accommodate the move operation. The thickness of the inner blue layer is twice that of the outer green layer in Fig. 7(a). The main reason is to insulate atoms of the inner layer from the interaction of atoms outside the outer layer.

4. The last step is to paste the surface together. The simplest way is to shift the atoms inside the hemispherical shell with the same amount of displacement vector. Indeed, the normal displacement of atoms on the loop plane is found negligibly small after the above simulation run. Afterwards, the discontinuity across the hemispherical cut disappears, while no new discontinuity arises. The paste operation is done by post-processing the dumped file containing atom information and thus no need for running additional simulation.
5. With the presence of void, the overall operation remains the same. The only difference is that hemispherical shells are missing a piece due to intersecting with the void in Fig. 7(c).

The only discontinuity left is the dislocation loop itself as seen in Fig. 7(b). The perfect shear loop dissociated into partial dislocations during the simulation in Figs. 7(b, d). The Burgers vector of the outer Shockley partial is 1/6[-1 -1 2], while 1/6[-2 1 1] for the inner one. They were dissociated from the perfect dislocation of a Burgers vector 1/2[-1 0 1]. This certainly makes sense, since the dissociated Shockley partials are more energetically favourable. The dislocation networks in Figs. 7(b, d) are calculated by the software ATOMVIEWER (Begau et al. 2012). We have confirmed them by using software OVITO (Stukowski 2010), which yielded exactly the same dislocation configuration as in Fig. 7. Figure 7(e) remarkably resembles that by using a flat cut in Fig. 5 of Dang et al. (2017) with small semi-major axis. They also found a smooth dissociated dislocation core as the result of energy minimization. Although the hemispherical cut is somehow arbitrarily chosen, the dislocation loop tends to be more circular once getting larger (Scattergood and Bacon 1974, Dang et al. 2017). In this work, not only a non-flat surface cut is applied, but also the image effect from the nearby void is involved. Even not regarding the mass transfer, the atomistic simulations dealing with arbitrary surface cut could shed some new light

on the discrete dislocation dynamics (DDD) simulation to reflect this arbitrariness.

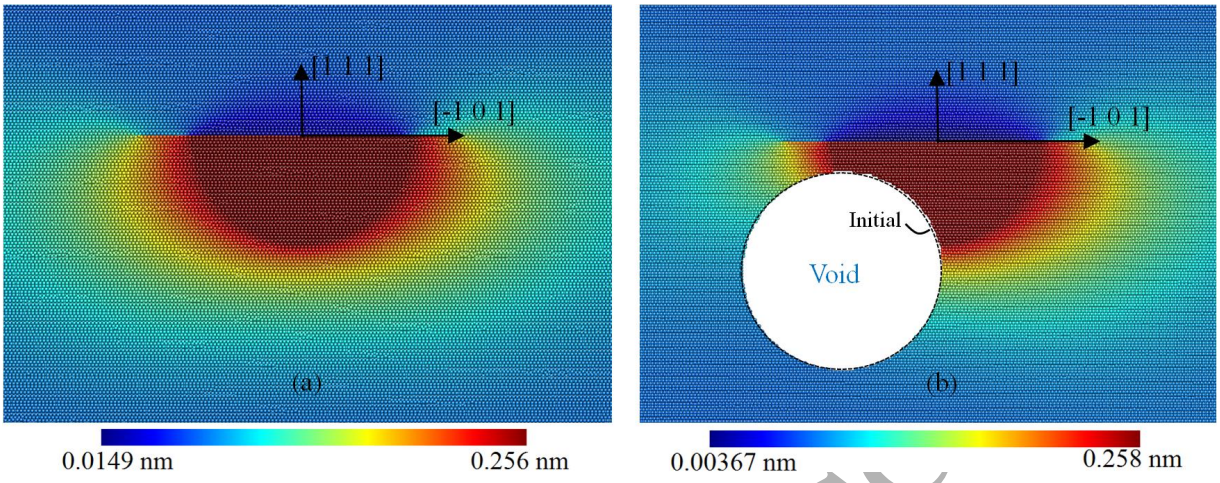

Fig. 8. Atomic displacement field (magnitude) as measured from initially dislocation-free configuration for (a) a standalone shear loop and (b) a shear loop generated near a void. The software ATOMEYE (Li 2003) is employed in plotting. The cutting plane for the 2-D plot is (1 -2 1). The dashed circle in (b) marks the initial void profile.

Table 2
Void growth due to the generation of a shear dislocation loop

	Void growth ratio ($\Delta V/V_0$)	
	Simulation	Theoretical, Eq. (24)
Hemispherical surface cut	1.275%	1.162%

Next to examine is the displacement field and void growth after introducing the dislocation loop. For the void-free case, the largest values are inside the hemispherical dome due to the paste operation. During the simulation run, elastic deformation builds up due to displacing the hemispherical shell as seen in Fig. 8(a). For the void-embedded case, part of the void surface is within the paste zone and hence acquires some growth. The initial void volume fraction for the dislocation-free state is 1.2766%. After the paste operation, the void volume fraction of the system rises to 1.2929% as a consequence of the hemispherical cut. The ratio of void growth can

be calculated by relating its incremental change to its initial volume as

$$\frac{\Delta V}{V_0} = \frac{\int_A \boldsymbol{b}\cdot\boldsymbol{n}\mathrm{d}S}{V_0}. \tag{24}$$

The surface A for the integral in Eq. (24) is the intersection area defined in Fig. 3(a). In the atomistic simulation, the way to paste the two sides of the cut together has to be specified. By comparison, Eq. (24) does not specify the way, as long as the cut is enclosed by the chosen control volume, as discussed in the preceding section. As listed in table 2, the atomistic simulation leads to a void growth ratio of 1.275% due to the hemispherical cut. By comparison, Eq. (24) yields a growth ratio of 1.162% by performing the integration on the intersected area of the void surface. The difference is apparently due to the additional elastic deformation.

3. The dynamic formation/emission

3.1 The new insight

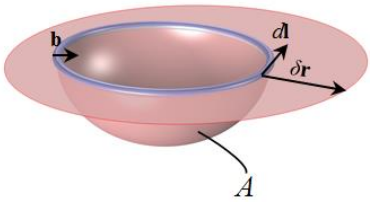

Fig. 9 Increment of A for the motion of a full shear loop (Hirth and Lothe 1982, Bower 2009)

It is true that once a dislocation loop is completed, the further conservative motion would not induce any new mass transfer. During the motion of a dislocation loop, surface elements $\delta\mathbf{A} = \delta\mathbf{r} \times d\mathbf{l}$ are added to the surface cut A that generates the loop in the first place. As seen in Fig. 9, neither the glide nor expansion of a full shear loop will induce further mass transfer since the additional $\delta\mathbf{A}$ would only be flat. This is exclusively valid for a complete loop, as stated in the textbooks (Hirth and Lothe 1982, Bower 2009). However, one might ask: is this truly inapplicable to dislocation segments? In other words, would the expansion and glide of

dislocation segments, before completing a loop, unable to induce mass transfer? Indeed, the dynamic expansion of incomplete shear loops as seen in MD simulation could be viewed as both: (1) the dynamic formation of new dislocation segments and (2) the gliding and expansion of the existing segments. We believe that this pivotal question can be answered by the proof by contradiction in Fig. 10.

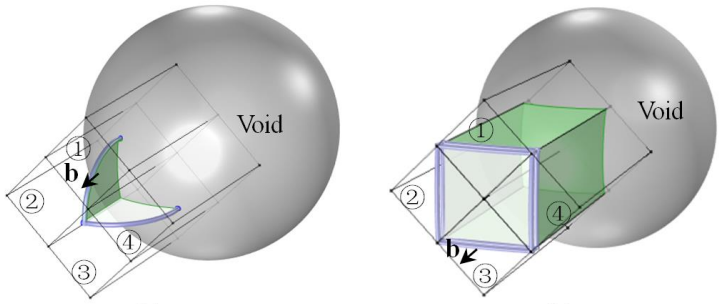

Fig. 10 Proof by contradiction: if the initiation, expansion and glide of dislocation segments were prohibited to grow voids, a prismatic loop in (b) evolved from (a) cannot grow voids either. Four control volumes ①②③④ disassemble the shear loop and the prismatic loop into only dislocation segments. Green planes are gliding planes instead of surface cuts.

The logic in Fig. 10 is simple: if the initiation, expansion and glide of dislocation segments were prohibited to transfer mass, the prismatic loop cannot grow voids either. The control volumes disassemble the loops into only dislocation segments in Fig. 10. During the V-shape shear loop evolves into a full prismatic loop, within each control volume, only the initiation, expansion and glide of dislocation segments are involved. If $\delta \boldsymbol{A}$ were flat for each segment in each control volume, the total A would always stay flat, which results in $\Delta V = 0$ for each control volume even after the completion of the prismatic loop in Fig. 10(b). That is to say, such a prismatic loop would also be prohibited to grow voids. This contradicts not only common understandings, but also experimental and MD observations. Indeed, in the upcoming subsection, we will rely on MD simulations for further confirmation. In short, Fig. 9 is inapplicable to

dislocation segments. The surface A until the completion of a dislocation loop should stay arbitrary and allow void growth. Furthermore, this amount of growth is not necessary to be forfeited upon the completion of a dislocation loop, as seen in Fig. 11(c). Obviously, the amount of growth $\int_A \boldsymbol{b}\cdot\boldsymbol{n}\mathrm{d}S \neq 0$ for the surface cut A in Fig. 11(c). In contrast, once completed, the shear loop will not induce further growth via gliding. In reality, a single, isolated full shear loop gradually leaving the void can be rare since multiple dislocations can be emitted simultaneously once critical stress is reached. Detached, yet interconnected faulted shear loops can be found in previous MD simulations (Cui and Chen 2016), whose mass transfer can be understood by the schematic in Fig. 11.

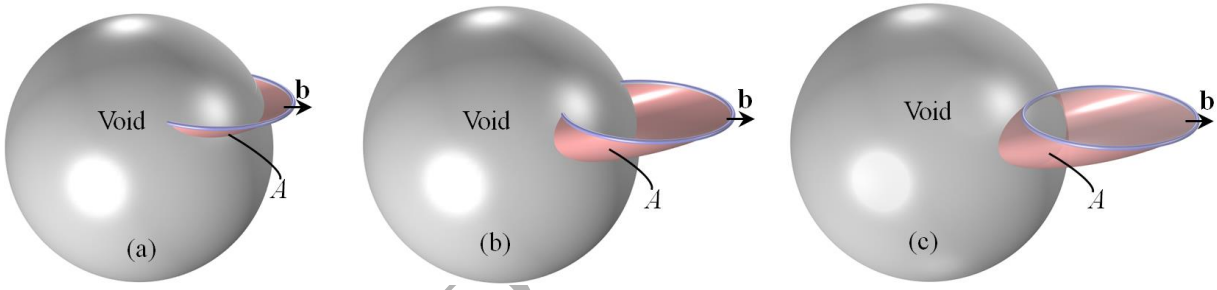

Fig. 11 The surface cut A that still grows a void upon completion of the shear loop. The transferred mass is not necessarily to be forfeited. After the completion, conservative motions (i.e. gliding or expansion) only add a flat increment to A and hence no further growth.

3.2 MD simulations

Although MD simulations of defective structure under tension or compression have been extensively reportedly (Traiviratana et al. 2008, Bringa et al. 2010, Tang et al. 2012, Krasnikov and Mayer 2015, Cui and Chen 2016, Cui and Chen 2017a, Xiang et al. 2017, Jing et al. 2018), we here offer new understanding from several aspects. First, although prismatic loops are known to induce mass transfer, the local mass redistribution associated with their transformation from shear loops has never been investigated. Neither has the mass transfer during the cross-slip of

shear loops, although these cross-slipped V-shape shear loops have already been studied in the MD simulation of nano-indentation long ago. Second, we will clarify that these V-shape shear loops are not necessary the precursors of prismatic loops and hence cannot be already deemed as prismatic loops. Third, the square-frustum structure of dislocation under uniaxial tension will be re-examined to clarify that they should not be counted as a dislocation loop with prismatic character. The triaxial tension case in subsection 3.2.1 is for the first aspect, while the uniaxial tension case in subsection 3.2.2 is for the second and third aspects. For the uniaxial tension, we focus on the V-shape shear loop and the disproof of its prismatic character, which has never been reported.

3.2.1 Prismatic loops formed by shear loops under triaxial tension

The void-embedded geometry is created by removing the copper atoms within a spherical region (r=3.615 nm) centered in a cubic simulation box (30.4nm×30.4nm×30.4 nm). The total atom count is approximately 2.4 million. The initial void volume fraction is 0.71%. The boundaries of the simulation box are made periodic for all three directions. A fixed time step of 1fs is applied throughout the simulation. Energy minimization is first performed by using a conjugate gradient algorithm to attain a minimum energy configuration, followed by a relaxation step to reach an equilibrium-state configuration under the designated temperature. The equal triaxial load with a strain rate of 2×10^{8} s^{-1} is then applied at all directions. The initial temperature for the dynamic run is 1K and no thermostat or barostat is applied. The MD post-processing software ATOMVIEWER (Begau et al. 2012) is employed in post-processing the MD data. It combines the modified Nye-tensor method and the dislocation line extraction method to derive Burgers vectors and dislocation network without constructing Burgers circuits explicitly. In general, the simulation results confirmed the established process of prismatic loops to form under

triaxial tension through cross-slip of shear loops (Tang et al. 2012). Yet, the mass transfer pattern, during and after the formation of prismatic loop, has rarely been examined. Hence, our attention is paid to the mass transfer only.

Under the equal-triaxial tension, the central void started to expand elastically and no any form of dislocation was seen until the strain reached the value of 1.94%. Incipient shear loops started to appear only after a strain of 2.36% and then developed rapidly into coordinated structures. The prevailing pattern is that Shockley partial dislocations grow on planes {111}, since they are more energetically favourable than perfect ones. In Fig. 12(a), highlighted dislocation segments belong to a shear loop during cross-slip, which later turns into a prismatic loop as also highlighted in Fig. 14(a). No prismatic loop was found in Fig. 12. The seemingly prismatic one is only a visual illusion, which actually involve a V-shape shear loop and another unrelated partial dislocation in the rear side.

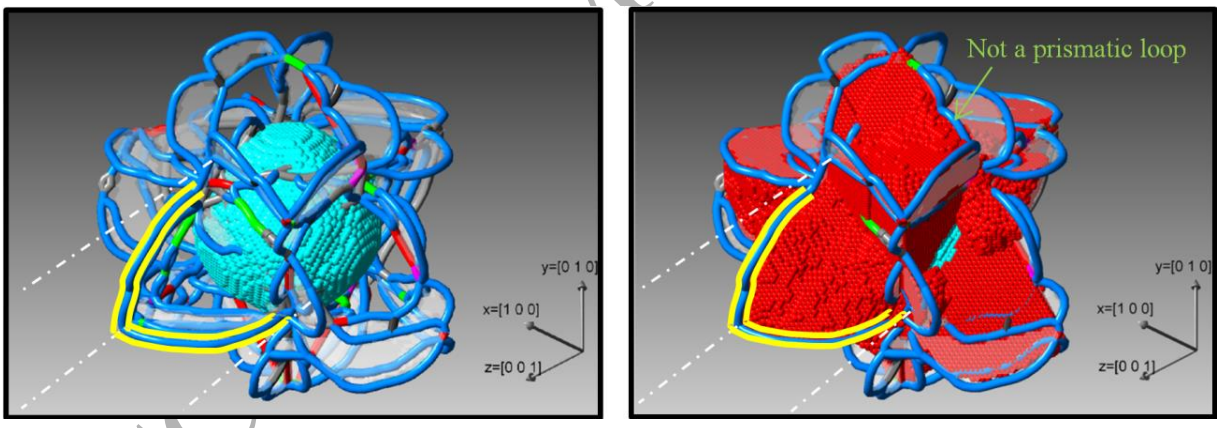

(a) Without RFT atoms (b) With RFT atoms

Fig. 12 Incomplete shear loops highlighted in yellow prior to prismatic loop formation at a strain of 2.484% and the corresponding mass transfer pattern. The light blue atoms in (a) represents void surface. The rendered lines are dislocations. The critical length for relatively farthest-travelled (RFT) atoms is 0.15 nm.

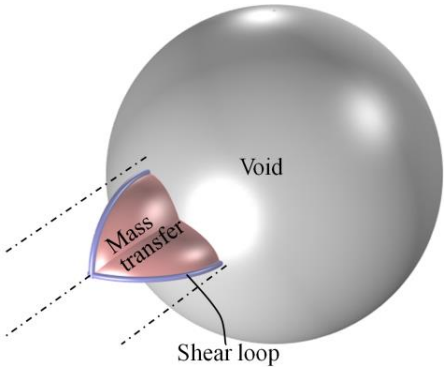

Fig. 13 Schematic drawing for mass transfer associated with an incomplete shear loop

Recall that we defined $[\boldsymbol{u^{Ext}}, \boldsymbol{\varepsilon^{Ext}}, \boldsymbol{\sigma^{Ext}}]$. Thus, the relative displacement actually excludes $\boldsymbol{u^{Ext} - u^{I}}$ from the total, where $\boldsymbol{u^{I}}$ is the image one. At the very least, the unwanted image one of the external load will not exaggerate the void growth, since this image stress offsets the tensile traction on void surface. The RFT atoms are identified once the relative displacements exceed some critical level. As an improvement, the end of elastic stage, instead of the unstrained system (Cui and Chen 2016), is taken as the reference configuration for better illustrations. In ATOMVIEWER, the simplest way to do so is to assign virtual element type to RFT atoms once they are identified and enable the show elements function. As expected, the RFT atoms in Fig. 14(b) correctly capture the mass transfer via the emission of prismatic loops, which could be taken as a validation of the method itself. The void growth, exactly as the classical understanding, can be induced by prismatic loops. The RFT atoms are enclosed in the prismatic cylinders swept by gliding prismatic loops. The leading RFT atoms ahead of the prismatic cylinder connect to the trailing partial dislocations. Based on the validation, RFT atoms in Fig. 12(b) confirm that shear loops can also induce mass removal/insertion. These RFT atoms in Fig. 12(b) are enclosed by the leading partials. Also, the fact that RFT atoms gather at one side of a certain slip plane rules out them being the elastic deformation, which should be antisymmetric with respect to the loop plane (Ohr, 1972). The schematic drawing in Fig. 13 describes that RFT

atoms could take a combined shape of the mass transfer region caused by two dislocation segments. Indeed, Eq. (21) states that the energy due to the work done to introduce the dislocation into external load, favours the surface cut that can grow void under a triaxial loading. It is not only true for the well-known void growth via prismatic loops, but also should be true for the void growth via shear loops.

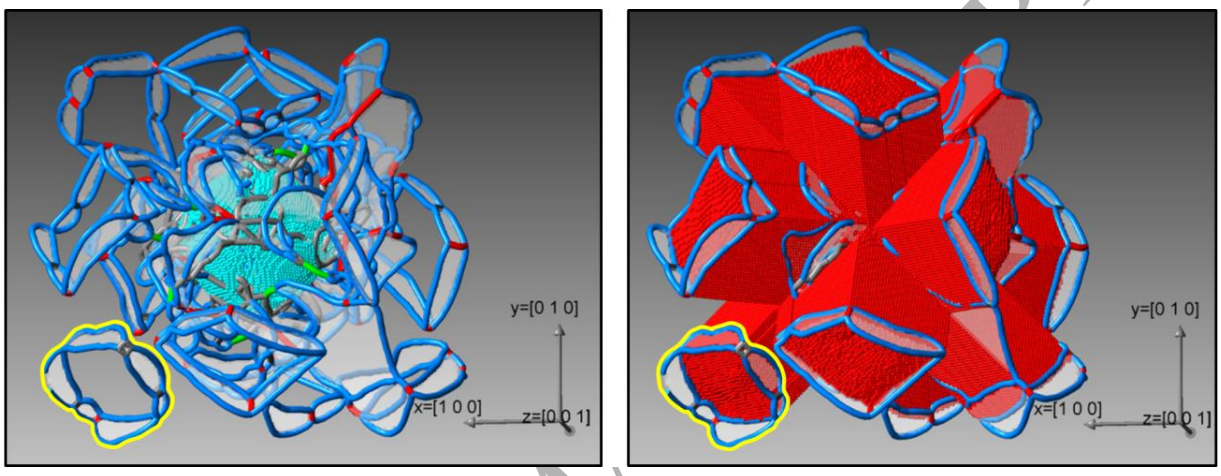

(a) Without RFT atoms (b) With RFT atoms

Fig. 14 Dislocation network formed at a strain of 2.592% around void under a triaxial tension and the mass transfer pattern during void growth. The highlighted prismatic loop evolved from the also highlighted shear loops in Fig. 12. Its slight opening is due to reaching the periodic boundary.

In Fig. 14, a total of 12 rows of prismatic loops are emitted, although some are unseeable in the rear side. Most of prismatic loops have detached from the void, although some still has its stacking fault area connected to the void.

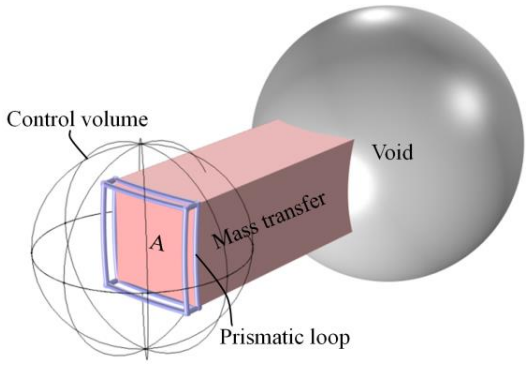

Fig. 15 Schematic drawing for mass transfer associated with prismatic loop

Fig. 15 depicts the mass transfer of a prismatic loop gliding away from the void, adapted from the MD simulation. The prismatic loop has not only formed but also glided to its current position. Assuming no climb is involved, the mass transport caused by the gliding motion of the prismatic loop can be evaluated as

$$\Delta V^*_{motion} = \oint_C \boldsymbol{b} \cdot (\delta \boldsymbol{r} \times \mathrm{d}\boldsymbol{l}) = 0. \tag{21}$$

The triple product in the above equation is obviously zero since the motion is a pure slip, i.e. these vectors $\boldsymbol{b}$, $\delta\boldsymbol{r}$ and $\mathrm{d}\boldsymbol{l}$ are in a same plane. Indeed, neither the conservative motion of a shear loop nor that of a prismatic loop can cause additional void growth. Hence, the concerned void growth exclusively comes from the formation.

$$\Delta V^*_{Void} = \Delta V^*_{formation} + \Delta V^*_{motion} = \Delta V^*_{formation} \tag{22}$$

Given this fact, the prismatic loop can be deemed as if formed at the current position for evaluating mass transfer. By choosing the control volume as shown in Fig. 15, its volumetric change can be calculated as

$$\Delta V^*_{formation} = \int_{V_{CV}} \varepsilon^*_{kk} \mathrm{d}V = -\int_A \boldsymbol{b} \cdot \boldsymbol{n} \mathrm{d}S \tag{23}$$

The minus sign indicates shrinkage of the control volume, which implies the growth of the void. We then reach a very interesting conclusion that the gliding of a prismatic loop, though causes no

further growth of void, is extending the effective mass transfer region into the material. Indeed, the motion of an edge dislocation can be visualized as a moving caterpillar, whose hump represents the added layer of atoms, is propelled away from the void due to the load.

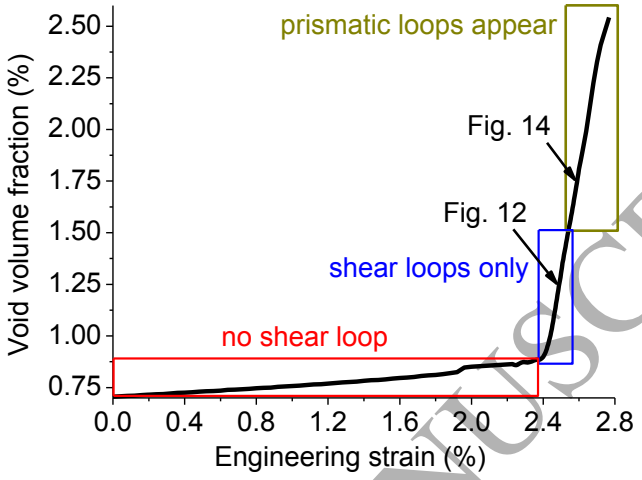

Fig. 16 Corresponding void volume fraction under triaxial tension.

In Fig. 16, the curve of void volume fraction versus strain certainly confirms the above findings. The void growth is almost linear and elastic with no shear loop present. The drastic increase of void size is triggered when there are only shear loops in the system. There is barely a change in the slope during the shift from shear loops only to prismatic loop's prevailing in Fig. 16. If shear loops were really unable to grow the void, the drastic change would rather be when prismatic loops are first formed. The void growth is a continuous process ever since the beginning of dislocation emission. The reason behind is simply that shear loops can grow the void. Near the end of the curve, the subsequent growth of void is due to a new round of shear loop emission and hence new prismatic loop emission.

3.2.2 The coordinated dislocation structure formed by shear loops under uniaxial tension

Although the simulation itself is similar to many previous works, we here only focus on the

V-shape shear loop and the disproof of its prismatic character. The loading here is with uniaxial strain. Only the x direction is stretched and lengths of the other two directions are fixed. The dislocation emission only occurs after a strain of 5.25% in Fig. 17(a). The emerging incomplete shear loops abruptly grow into coordinated square-frustum structure as seen in Fig. 17(b). As seen in Table 3, the leading and trailing partial dislocations farthest away from the void in Fig. 17(b) do not constitute a dislocation loop. Apparently, their Burgers vectors of supposed perfect dislocations if undissociated are not the same. Unlike a prismatic loop spanning two slip planes, these leading and trailing partials are in four slip planes. According to the last row in Table 3, only segments 3 and 4 have the same Burgers vector if undissociated. Hence, they constitute a V-shape shear loop. However, this V-shape shear loop has never turned into a prismatic loop. Therefore, V-shape shear loops are not necessarily precursors of prismatic loops. Void growth occurs with only shear loops in the system.

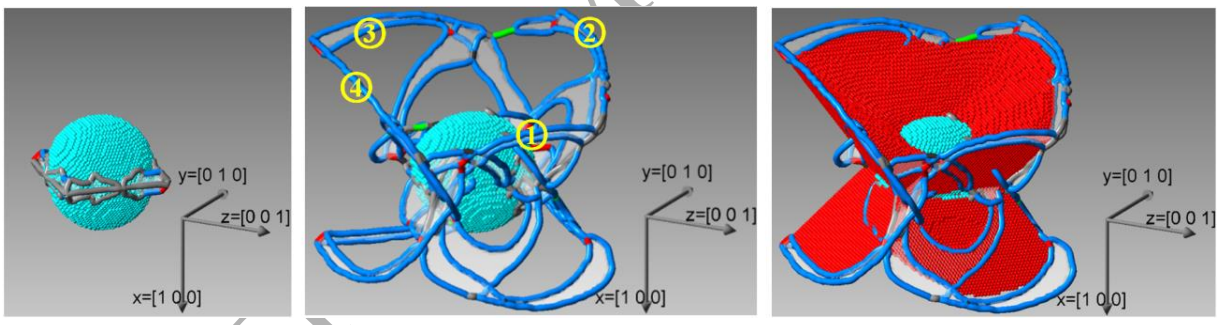

(a) strain=5.25% (b) strain=5.4% (c) strain =5.4% (with RFT atoms)

Fig. 17 Dislocation network around void under uniaxial tension and the mass transfer pattern during void growth. The light blue atoms in (a) represents void surface. The rendered lines are dislocations. The critical length to identify RFT atoms is 0.15 nm. Figure (a) is used as the reference configuration for RFT atoms.

Table 3

The Burgers vectors of the dislocation segments marked inside Fig. 17(b)

Dislocation segment:	1	2	3	4
Slip plane	(-1 1 -1)	(-1 -1 -1)	(-1 -1 1)	(-1 1 1)
b of the leading partial	1/6[-1 1 2]	1/6[-1 2 -1]	-1/6[1 1 2]	1/6[-1 1 -2]
b of the trailing partial	1/6[-2 -1 1]	1/6[-2 1 1]	1/6[-2 1 -1]	-1/6[2 1 1]
b if undissociated	1/2[-1 0 1]	1/2[-1 1 0]	-1/2[1 0 1]	-1/2[1 0 1]

The prevailing dislocations in the system are still Shockley partials. Unlike the triaxial-tension case, prismatic loop has never been observed. For the dynamic emission of shear loops and their coordinated structure, the caterpillar analogy of dislocation motion is still helpful. The mass transfer region is expanding and extending with the growth of leading partial dislocation. The dislocation segments of the square-frustum structure are not only gliding but also gaining length. Due to the arbitrary surface cut, their formation is responsible for the mass transfer and hence void growth. Without the completion of prismatic loop, the void growth is dominated by shear loops and their coordinated structure. In Fig. 12, the initial void growth is almost linear and elastic. The drastic growth of void size occurs only after the formation of incomplete shear loops. Unlike the triaxial-tension case, only incomplete shear loops are seen and no prismatic loop is observed. As marked in Fig. 12, the count of non-closed shear loops increases from initially 6 to 26 when some of them reach periodic boundaries. The highlighted V-shape shear loop in Fig. 17 is among the first few emitted and contributes substantially to the gain of void volume. With no prismatic loop ever completed, void growth is still a continuous process due to the multiplication of non-closed shear loops and their coordinated structure as seen in Fig. 18. Since there is no closed loop, Eq. (21) for evaluating mass transfer of a moving, closed dislocation loop by definition is not applicable and hence cannot invalidate this growth mechanism by non-closed loops. Also, direct or indirect evidence of void growth via shear loops in MD simulation can be found in the literatures (Traiviratana et al. 2008, Bringa et al. 2010, Tang et al. 2012, Krasnikov and Mayer 2015, Cui and Chen 2016, Cui and Chen 2017a, Xiang et al. 2017, Jing et al. 2018).

Void growth via incomplete shear loops were observed when thermo-mechanical constraints, strain rates, simulation sizes (Cui and Chen 2017c, Cui and Chen 2018) and even initial void shape (Cui and Chen 2015a, 2015b) were altered. Nonetheless, there could be occasions that incipient shear loops have little influence in mass transfer, probably concerning the way of loading. For instance, the formation of incipient shear loops barely affected the decreasing porosity of the nanoporous metal under uniaxial compression (Cui and Chen 2017b). After all, the cut to create dislocation loops can be arbitrary, depending on the situation.

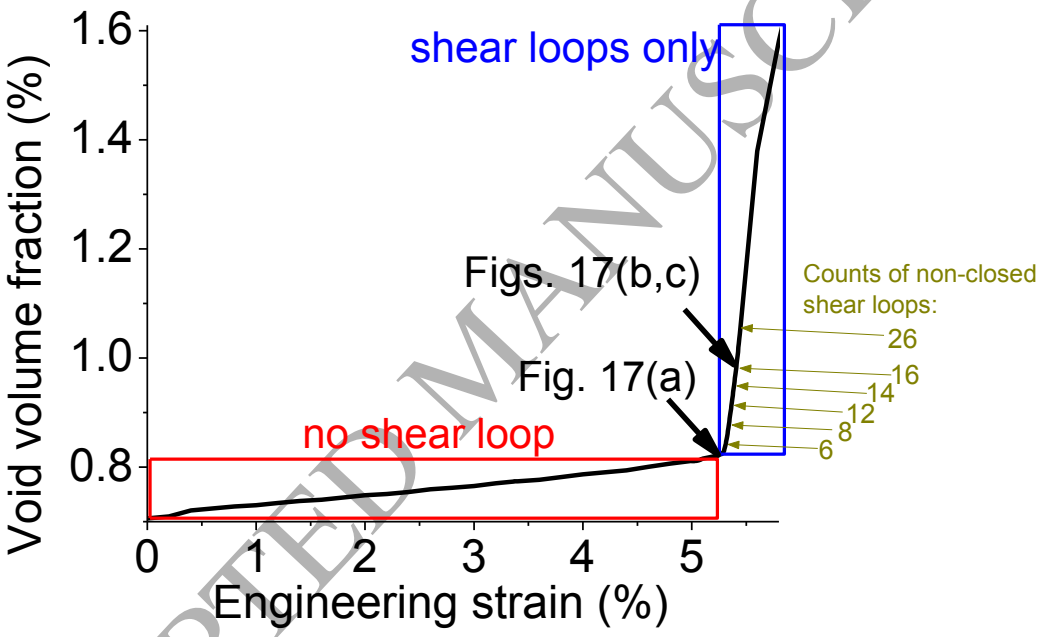

Fig. 18 Corresponding void volume fraction under uniaxial tension.

4. Conclusions

We combine the molecular statics, nonsingular dislocation theory, finite element method and molecular dynamics approach to offer new insights into the mass transfer regarding geometrically-necessary dislocations. Our major findings are as follows, which answer those challenges mentioned in the introduction.

1. We prove that the generation of full shear loops, not only incomplete ones, can also grow

voids

2. Among all possible cuts, the potential energy could favour the one that grows the nearby void under triaxial tension.
3. An approach via MD simulation adapted from the "cut, displace and paste" operation has been established, which, for the first time, successfully creates a shear dislocation loop via a hemispherical cut.
4. Through proof by contradiction, we show that surface cuts of dislocation segments during dynamic emission should stay arbitrary. The transferred mass by a full shear loop is not necessarily to be forfeited upon its completion. The V-shape shear loops can already induce mass transfer before turning into prismatic loops under the triaxial tension. Rather, it is the prismatic loop that later "inherits" this ongoing mass transfer.
5. We reveal that the leading dislocations at the opening of coordinated dislocation structures should not be mistaken as a loop with prismatic character. These V-shape shear loops under the uniaxial tension never turned into prismatic loops until the end of loading. Most of them form square frustum-like dislocation structure. It can at least be sure that V-shape shear loops are not necessarily precursors of prismatic loops. They grow voids only because that their surface cuts can be arbitrary.

Acknowledgments

We acknowledge the computing resources and technical support from the Western Canada Research Grid (WestGrid). Financial support for this work has been provided by the Natural Sciences and Engineering Research Council of Canada (NSERC), and is gratefully acknowledged.

Reference

Begau, C., Hua, J., Hartmaier. A., 2012. A novel approach to study dislocation density tensors and lattice rotation patterns in atomistic simulations. J. Mech. Phys. Solids. 60, 711-722

Bower, A.F., 2009. Applied mechanics of solids. CRC Press, Boca Raton, 359-364

Bringa, E.M., Traiviratana, S., Meyers, M.A., 2010. Void initiation in fcc metals: Effect of loading orientation and nanocrystalline effects. Acta Mater. 58, 4458-4477.

Bringa, E.M., Monk, J.D., Caro, A., Misra, A., Zepeda-Ruiz, L., Duchaineau, M., Abraham, F., Nastasi, M., Picraux, S.T., Wang, Y.Q., Farkas, D., 2011. Are Nanoporous Materials Radiation Resistant? Nano Lett. 12, 3351-3355.

Bulatov, V.V., Wolfer, W.G., Kumar, M., 2010. Shear impossibility: Comments on "Void growth by dislocation emission" and "Void growth in metals: Atomistic calculations", Scr. Mater. 63, 144-147.

Cai,W., Arsenlis, A., Weinberger, C.R., Bulatov, V.V., 2006. A non-singular continuum theory of dislocations. J. Mech. Phys. Solids. 54, 561-587.

Cui, Y., Chen. Z., 2015a. Molecular dynamics simulation of the influence of elliptical void interaction on the tensile behavior of aluminum. Comput. Mater. Sci. 108, Part A, 103-113

Cui, Y., Chen. Z., 2015b. Molecular dynamics modeling on the role of initial void geometry in a thin aluminum film under uniaxial tension. Modell. Simul. Mater. Sci. Eng. 23, 085011

Cui, Y., Chen. Z., 2016. Material transport via the emission of shear loops during void growth: A molecular dynamics study. J. Appl. Phys. 119, 225102

Cui, Y., Chen. Z., 2017a. Void initiation from interfacial debonding of spherical silicon particles inside a silicon-copper nanocomposite: A molecular dynamics study. Modell. Simul. Mater. Sci. Eng., 25, 025007

Cui, Y., Chen. Z., 2017b. Simulation of mechanical performance of nanoporous FCC copper under compression with pores mimicking several crystalline arrays. J. Appl. Phys. 122, 075102.

Cui, Y., Chen. Z., 2017c. Void growth via atomistic simulation: will the formation of shear loops still grow a void under different thermo-mechanical constraints? Philos. Mag. 97, 3142-3171

Cui, Y., Chen. Z., 2018, New mechanisms of helical dislocation formation via the pinch-off process near a nano-inhomogeneity. Comput. Mater. Sci. 155, 400-409.

Dang, K., Capolungo L., Spearot, D. E., 2017. Nanoscale dislocation shear loops at static equilibrium and finite temperature. Model. Simul. Mater. Sci. Eng. 25, 085014.

Hirth, J.P., Lothe, J., 1982. Theory of Dislocations. second ed., Krieger, Malabar, FL, 96–97

Jing, P., Yuan, L., Shivpuri, R., Xu, C., Zhang, Y., Shan, D., Guo, B., 2018. Evolution of spherical nanovoids within copper polycrystals during plastic straining: Atomistic investigation. Int. J. Plast. 100, 122-141.

Krasnikov, V.S., Mayer, A.E., 2015. Plasticity driven growth of nanovoids and strength of aluminum at high rate tension: Molecular dynamics simulations and continuum modeling. Int. J. Plast. 74, 75-91.

Landau, L.D., Lifshitz. E.M., 1970. Theory of elasticity; 3rd ed., Butterworth-Heinemann, Oxford, 1970, 111-112

Li, J., 2003. AtomEye: an efficient atomistic configuration viewer. Modell. Simul. Mater. Sci. Eng. 11, 173

Li, S., Li, Y., Lo, Y., Neeraj, T., Srinivasan, S., Ding, X., Sun, J., Qi, L., Gumbsch P., Li Ju., 2015. The interaction of dislocations and hydrogen-vacancy complexes and its importance for deformation-induced proto nano-voids formation in a-Fe. Int. J. Plast. 175-191.

Lubarda, V.A., Schneider, M.S., Kalantar, D.H., Remington, B.A., Meyers, M.A., 2004. Void growth by dislocation emission. Acta Mater., 52, 1397-1408.

Lubarda, V.A., 2011. Emission of dislocations from nanovoids under combined loading. Int. J. Plast. 27, 181-200.

Meng, F., and Jin, S., 2011. The Solution Growth of Copper Nanowires and Nanotubes is Driven by Screw Dislocations. Nano lett. 12, 234-239

Mishin, Y., Mehl, M.J., Papaconstantopoulos, D.A., Voter A.F., Kress, J.D., 2001. Structural stability and lattice defects in copper: Ab initio, tight-binding, and embedded-atom calculations. Phys. Rev. B 63, 224106.

Narayan, J., Washburn, J., 1972, Stability of dislocation loops near a free surface. 43, 4862-4865.

Zhou, X., Ward, D.K., Wong, B.M., Doty, F.P., Zimmerman, J.A., 2012. Molecular Dynamics Studies of Dislocations in CdTe Crystals from a New Bond Order Potential. J. Phys. Chem. C 116, 17563-17571

Ohr, S.M., 1972. Displacement field around a shear dislocation loop. Philos. Mag. 26, 1307-1312

Potirniche, G.P., Horstemeyer, M.F., Wagner, G.J., Gullett P.M., 2006. A molecular dynamics study of void growth and coalescence in single crystal nickel. Int. J. Plast. 22, 257-278.

Salehinia, I., Bahr, D.F., 2014. Crystal orientation effect on dislocation nucleation and multiplication in FCC single crystal under uniaxial loading. Int. J. Plast. 52, 133-146.

Scattergood, R.O., and Bacon, D.J., 1974. Dislocation shear loops in anisotropic crystals. Phys. Status Solidi 25 395–404

Sharma, P., Ganti, S., Bhate, N., Effect of surfaces on the size-dependent elastic state of nano-inhomogeneities. 2003. Appl. Phys. Lett., 82 (4), 535-537.

Spearot, D.E., Jacob, K.I., McDowel, D.L., 2007. Dislocation nucleation from bicrystal interfaces with dissociated structure. Int. J. Plast. 23, 143-160.

Stukowski, A., 2010. Visualization and analysis of atomistic simulation data with OVITO - the Open Visualization Tool. Modell. Simul. Mater. Sci. Eng. 18, 015012

Tang, Y., Bringa, E.M., Meyers, M.A., 2012. Ductile tensile failure in metals through initiation and growth of nanosized voids. Acta Mater. 60, 4856-4865

Traiviratana, S., Bringa, E.M., Benson D.J., Meyers, M.A., 2008. Void growth in metals: Atomistic calculations. Acta Mater. 56, 3874-3886.

Tschopp, M.A., McDowell, D.L., 2008. Dislocation nucleation in Σ3 asymmetric tilt grain boundaries. Int. J. Plast. 24, 191-217.

Xiang,M., Cui, J., Yang, Y., Liao, Y., Wang, K., Chen, Y., Chen, J., 2017. Shock responses of nanoporous aluminum by molecular dynamics simulations. Int. J. Plast. 97, 24-45.

Zhao, Y., Fang, Q., Liu, Y., Zeng, X., 2014. Dislocation emission from nanovoid with the effect of neighboring nanovoids and surface stresses. Int. J. Solids Struct. 51(7-8), 1617-1629.